chemistry

MDPI

Article

Sweet, Sugar-Coated Hierarchical Platinum Nanostructures for Easy Support, Heterogenization and Separation

Dennis Woitassek [1,†], José G. Moya-Cancino [1,†], Yangyang Sun [1], Yefan Song [1], Dennis Woschko [1], Stefan Roitsch [2] and Christoph Janiak [1,*]

[1] Institut für Anorganische Chemie und Strukturchemie, Heinrich-Heine-Universität Düsseldorf, 40204 Düsseldorf, Germany
[2] Institut für Physikalische Chemie, Universität zu Köln, 50939 Köln, Germany
* Correspondence: janiak@uni-duesseldorf.de; Tel.: +49-2118112286
† These authors contributed equally to this work.

Abstract: Metal nanoparticles are increasingly gaining interest in the field of heterogeneous catalysis. Here, we present a novel strategy for synthesizing sugar-coated platinum nanostructures (SC-Pt-NS) from the carbohydrates sucrose and D(-)-fructose. In the synthesis from a mixture of $H_2PtCl_6 \cdot 6H_2O$, the carbohydrate in an ionic liquid (IL) yielded primary particles of a homogeneous average size of ~10 nm, which were aggregated to hierarchical Pt nanostructures of ~40–65 nm and surrounded or supported by the carbohydrate. These sugar-coated platinum nanostructures present a facile way to support and heterogenize nanoparticles, avoid leaching and enable easier separation and handling. The catalytic activity of the SC-Pt-NS was shown in the hydrosilylation test reaction of phenylacetylene with triethylsilane, where very high turnover frequency (TOF) values of up to 87,200 h^{-1} could be achieved, while the platinum metal leaching into the product was very low.

Keywords: ionic liquids; platinum; carbohydrates; hierarchical nanostructures; supported nanoparticles; hydrosilylation; sugar; saccharide

Citation: Woitassek, D.; Moya-Cancino, J.G.; Sun, Y.; Song, Y.; Woschko, D.; Roitsch, S.; Janiak, C. Sweet, Sugar-Coated Hierarchical Platinum Nanostructures for Easy Support, Heterogenization and Separation. *Chemistry* **2022**, *4*, 1147–1160. https://doi.org/10.3390/chemistry4040078

Academic Editors: Gianguido Ramis and Alessandra Puglisi

Received: 5 August 2022
Accepted: 26 September 2022
Published: 30 September 2022

1. Introduction

An important aspect of metal nanoparticles (M-NPs) is their application in heterogeneous catalysis due to their high surface-area-to-mass or volume ratio [1–3]. The smaller the NP size, the larger the (active) surface area is, and the larger the specific catalytic activity of the NP catalysts should be. The main problem of very small M-NPs under catalytic reaction conditions is that they experience coalescence, aggregation, sintering or Ostwald ripening, which leads to the formation of larger and more stable but less active particles. To avoid this loss of catalytic activity, M-NPs must be stabilized, for instance, by capping ligands [4–6], surrounding polymers [7], coating in ionic liquid media [8,9] or by depositing them on supports, such as zeolites [10,11], carbon nanotubes [2] or reduced graphene oxide [12]. An intriguing extension of the well-known polyol synthesis of metal nanoparticles [13,14] and of a biogenic "green synthesis" of M-NPs using plant extracts [15–17] is the use of "sugars"; that is, carbohydrates as well-defined, cheap and also effective reducing and stabilizing agents [4–6]. Polyols, similar to ethylene glycol, propylene glycol, glycerol and poly(vinyl alcohol), have long been known as reducing agents in M-NP synthesis [18] and, at the same time, provide the needed stabilization [13,14]. Versatile and widely available carbohydrates [6,19] can be used as reducing, stabilizing and capping agents, fulfilling multiple roles simultaneously during synthesis [4,5]. Modified carbohydrates could control the size and shape of gold and silver nanostructures [4], and sugar-capped gold nanoparticles have been used for medical applications [20,21] and as sensors [22]. To the best of our knowledge, sugars were only reported twice and only as reducing agents in connection with Pt-NPs [23,24], and they have not been utilized as a support for Pt-NPs. We are not aware of saccharide coatings being used for catalytically active nanoparticles at large. Upon

mild decomposition of the carbohydrate, such as caramelization, the formed polymeric carbohydrates may also be used as in situ support material [19].

To reach a sufficiently high reaction temperature, and to use microwave-induced heating, an ionic liquid (IL) can be used as a reaction medium. ILs are salts with a melting point below 100 °C, commonly being liquid at room temperature [25–28] and often stable up to 200 or even 300 °C at least for a short reaction time [12,29–31]. ILs have a high absorption efficiency for microwave irradiation, which results in rapid and effective heating [12,32,33]. ILs are already used to synthesize M-NPs from a metal precursor [12,34–37] and are suitable stabilizers for M-NPs, owing to their high polarity, high ionic charge and dielectric constant. Further, imidazolium ILs can act as mild reducing reagents through the slightly acidic C-H atoms on the imidazolium ring.

Platinum on carbon in many forms, such as graphite, "graphene" and reduced graphite oxide, is already well-established. We have chosen saccharides (sugars), with the examples of sucrose and D(-)-fructose, due to the high amount of alcoholic groups found in sugars, enabling them to react as mild reducing agents for the synthesis of metal nanoparticles. Here, we present the synthesis of Pt-NPs by the reduction of $H_2PtCl_6{\cdot}6H_2O$ with saccharides in an IL medium and the in situ formation of a sugar (carbohydrate) coating or support as a stabilizer. This results in well-dispersed hierarchical sugar-coated Pt-nanostructures whose catalytic activity is shown as a proof of principle in the hydrosilylation reaction of phenylacetylene with triethylsilane (Scheme 1). We show that the sugar-coated platinum nanostructures have good stability under the catalytic conditions, the heterogenized catalyst composite can be easily separated from the product, and platinum leaching is prevented.

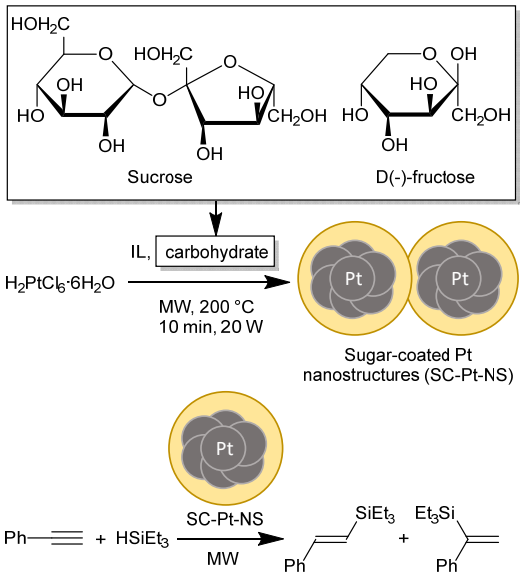

Scheme 1. Reaction conditions for the synthesis of sugar-coated Pt nanostructures (SC-Pt-NS) with the carbohydrates D-(-)-fructose and sucrose via microwave-induced heating in ionic liquid (IL) and subsequent catalytic hydrosilylation reaction.

2. Materials and Methods

2.1. Chemicals and Equipment

All starting materials and solvents were obtained from commercial sources and used as delivered (Table S1, Supplementary Materials). The IL 1-butyl-3-methylimidazoliumbis (trifluoromethylsulfonyl)imide ([BMIm]NTf_2) was synthesized using 1-chlorobutane, 1-methylimidazole and lithium bis(trifluoromethanesulfonyl)imide as precursors, following the approach presented by Cravotto et al. [38]. The IL purity was ascertained with ^1H and ^{13}C nuclear magnetic resonance (NMR) and ion chromatographic measurements (IC) (Figures S1 and S3).

A CEM-Discover SP lab microwave set-up with a power range of 0–300 W (±30 W) was used for the microwave-induced heating.

IC was carried out using a Dionex ICS 1100 instrument with suppressed conductivity detection. The suppressor (AERS 500, Dionex) was regenerated with an external water module. The system was equipped with the analytical column IonPac AS 22 from Dionex (4 × 250 mm) with the corresponding guard column AG 22 (4 × 50 mm). The instrument was controlled by Chromeleon® software (version 7.1.0.898). The injection volume was 25 µL. The standard eluent used was a 4.5 mmol L^{-1} Na_2CO_3 + 1.0 mmol L^{-1} $NaHCO_3$ mixture with an addition of 30 vol% acetonitrile (ACN).

Powder X-ray diffractograms (PXRDs) were measured with a Bruker D2 Phaser using a flat, low-background Si sample holder with Cu-Kα radiation (λ = 1.541874 Å, 35 kV). The scan time from 5 to 100° 2-theta was 1 h (1.58° min^{-1}). The program Diffrac.Eva V4.2 was used to evaluate the PXRD data.

Transmission electron microscopy (TEM) measurements were performed with a JEOL-2100 Plus and a Zeiss LEO912 at 200-kV and 120-kV accelerating voltages, respectively. The samples were prepared using 200-µm carbon-coated copper grids. Briefly, 0.05 mL of the SC-Pt-NS/IL dispersion after synthesis was dissolved in a 0.5-mL can, and one drop of the diluted dispersion was placed on the grid. After 30 min, the grid was washed with 3 mL ACN and air dried. The images were analyzed by Gatan Microscopy Suite version 3.3.

The NMR spectra were obtained on a Bruker Avance III 300 MHz-NMR in $CDCl_3$. The spectra were referenced on the residual solvent peak versus TMS (^{1}H NMR δ = 7.26 ppm for $CHCl_3$, ^{13}C NMR δ = 77.16 ppm for $CHCl_3$).

Gas chromatographic (GC) separations were performed with a Thermo Finnigan Trace GC Ultra, Column BPX5 (column length: 15 m), combined with the mass spectrometer (MS) Thermo Finnigan Trace DSQ, the EI ionization method, 70 eV and a source temperature of 200 °C.

Elemental analysis measurements of carbon, hydrogen, nitrogen and sulfur (CHNS) were performed with an Elementar Vario MICRO cube.

Fourier-transform infrared (FT-IR) spectrometry was performed on a Bruker Tensor 37 equipped with an ATR unit (Platinum ATR-QL, diamond) in the range from 4000 cm^{-1} to 550 cm^{-1} with a 2 cm^{-1} resolution (16 scans per measurement).

Thermogravimetric analysis (TGA) was performed with a Netzsch TG 209 F3 Tarsus device equipped with an Al crucible applying a heating rate of 5 °C min^{-1} under a synthetic air atmosphere.

Flame or graphite furnace atomic absorption spectrometry (F- or GF-AAS) measurements were performed on a Perkin Elmer PinAAcle 900T spectrometer. Sample masses were chosen to achieve a theoretical value in the calibration range of the AAS (5–30 mg_{Pt} L^{-1}). The carefully weighed samples were refluxed in aqua regia (10 mL), and the solvent evaporated at 120 °C until only a small amount of the solution was left. The residue was redissolved with aqua regia, and the procedure was repeated two more times. After the third evaporation, the residual solution was diluted with millipore water to the exact volume of 20 mL, from which 0.5 mL was taken and mixed with 2 mL of lanthanum standard solution and 0.05 mL hydrochloric acid before being diluted to a 10 mL volume with millipore water for the measurement. For the F-AAS, solutions of 5–30 mg_{Pt} L^{-1} (in 5-mg_{Pt} L^{-1} steps) from an AAS Pt standard (Fluka, 1000 ± 4 mg L^{-1}, 5% HCl) containing 2 mL of lanthanum standard were prepared for calibration. For the analysis of Pt leaching or residues after catalysis, graphite furnace atomic absorption spectrometry (GF-AAS) was utilized. A sample of 0.2 mL of the product solution was collected and diluted with ethanol to 1 mL. For GF-AAS, the calibration standards were 0.050 mg_{Pt} L^{-1}, 0.100 mg_{Pt} L^{-1} and 0.200 mg_{Pt} L^{-1} and were prepared from the same AAS Pt standard.

The optical activities were measured with a Polarimeter 341LC (Perkin Elmer) using a Na/Hal lamp at 589 nm and a path length of 100 mm. The samples were measured at

room temperature with a concentration of 0.7 mg mL^{-1}, with the exception of heat-treated D(-)-fructose with a concentration of 0.35 mg mL^{-1}.

MALDI-TOF mass spectrometry was performed with a MALDI-TOF/TOF UltraflX-treme (Bruker Daltonics) with 2,5-dihydroxybenzoic acid (gentisic acid, DHB) as a matrix.

GPC measurements were performed with a modular system from hs-GmbH. A VE 3580 RI Detector (Viscotek) was equipped with three columns (polystyrene, 10 × 8.0 nm, 5 µm; polystyrene, 300 × 8.0 nm, 5 µm; polyacryl, 300 × 8.0 nm, 5 µm) which were heated in a column oven at 60 °C. An S5250 sample injector (Sykam) as an auto-sampler was utilized. Polystyrene standard solutions (1280–1,373,000 g mol^{-1}) were used for calibration and dimethylformamide, containing LiBr (2.2 µg mL^{-1}) as a solvent. The measurements were carried out with an injection volume of 100 µL at a flow rate of 1 mL min^{-1}. The molecular weights were determined with the software Chromatographica (hs GmbH).

DLS measurements were performed with a Nano S Zetasizer (Malvern, Germany) equipped with a HeNe laser. The hydrodynamic radius was determined at a wavelength of 633 nm. Three measurements with an automatically decided number of runs were performed per sample. The sample was dispersed in chloroform. We want to point out that the detected compounds did not contain a spherical form and as such influence the resulting hydrodynamic radius.

2.2. Synthesis of Sugar-Coated Pt Nanostructures (SC-Pt-NS)

The general synthesis was performed well for the preparation of sample S25 (sucrose) and did not differ for the other sugar-coated Pt nanostructure (SC-Pt-NS) samples. The Pt precursor $H_2PtCl_6 \cdot 6H_2O$ (20.0 mg, 0.04 mmol) and sucrose ($C_{12}H_{22}O_{11}$, 22.6 mg, 0.07 mmol) were mixed in 0.94 g (0.65 mL) of the IL [BMIm]NTf_2. The mixture was stirred for 2 h at 400 rpm, followed by microwave heating for 10 min at 200 °C under 20 W of microwave power. By the addition of 3 mL of acetonitrile and centrifugation at 4000 rpm for 10 min, a solid product was separated from the brown solution. The washing process using acetonitrile was repeated several times until after 6–8 washing cycles with a total of 18–24 mL of acetonitrile, a colorless solution was obtained. Finally, the solid product was dried at room temperature in an oil pump vacuum. Similarly, D(-)-fructose ($C_6H_{12}O_6$) was reacted with $H_2PtCl_6 \cdot 6H_2O$. The Pt loading has to be determined post-synthetically by AAS as it differs from the initial Pt/carbohydrate ratio. The sample designation was based on the letter "S" or "F" for the used carbohydrate of sucrose and fructose, respectively, and the rounded found Pt wt.% from AAS. Samples S13, S25 (both from sucrose), F14 and F32 (both from D(-)-fructose), which had Pt contents of 12.8 wt.%, 24.7 wt.%, 13.6 wt.% and 31.5 wt.%, respectively, were selected for further analysis, while other samples are only given in the Supplementary Materials (Section S3). For comparison purposes, unsupported Pt-NPs were synthesized following identical experimental steps but without the presence of a carbohydrate (Section S7).

2.3. Hydrosilylation Reactions

The batch catalytic reactions were performed in a microwave reactor set-up using quartz glass vials of 10 mL. A mixture of an exactly weighed 1-mg SC-Pt-NS catalyst, 1 mg $H_2PtCl_6 \cdot 6H_2O$ or 1 mg of (sugar-free) Pt-NPs (see Section S9), 0.54 mL (4.9 mmol) of phenylacetylene and 0.79 mL (4.9 mmol) of triethlylsilane was placed in the glass reactor, followed by a reaction at 200 °C for 5 min under 200 W of microwave irradiation. The product solution was collected after centrifugation and analyzed by ^{1}H NMR, ^{13}C NMR and GC. The different product species were identified and quantified, and the conversion was derived.

3. Results

3.1. Synthesis and Characterization

Sugar-coated platinum nanostructures (SC-Pt-NS) were synthesized by the reduction of hexachlorido (formerly hexachloro)-platinic acid hexahydrate ($H_2PtCl_6 \cdot 6H_2O$) with

the saccharidessucrose (S) or D(-)-fructose (F) as reducing agents in the IL [BMIm]NTf_2 at 200 °C. The characterization of [BMIm]NTf_2 is presented in Section S2. Polyols are frequently used as reducing and stabilizing agents for the synthesis of metal nanoparticles. Moreover, reaction products from heat treatment of the saccharides could result in small vesicles inside the IL, promoting the formation of structured nanoparticle aggregates at these vesicles. While the amounts of $H_2PtCl_6 \cdot 6H_2O$ and IL were kept constant, the amount of sugar was varied to give sucrose-Pt samples with Pt contents between 4.7 and 24.7 wt.%, which were designated as S5–S25. For the fructose-Pt samples, the Pt fraction varied between 5.7 and 31.5 wt.%, with the samples named as F6–F32. The Pt content was post-synthetically determined by atomic absorption spectrometry (AAS). From the powder X-ray diffraction (PXRD) analysis, the formation of metallic Pt was confirmed in all samples with average crystallite sizes from the Scherrer equation between 8 and 12 nm (Figure 1 and Table S2, Supplementary Materials).

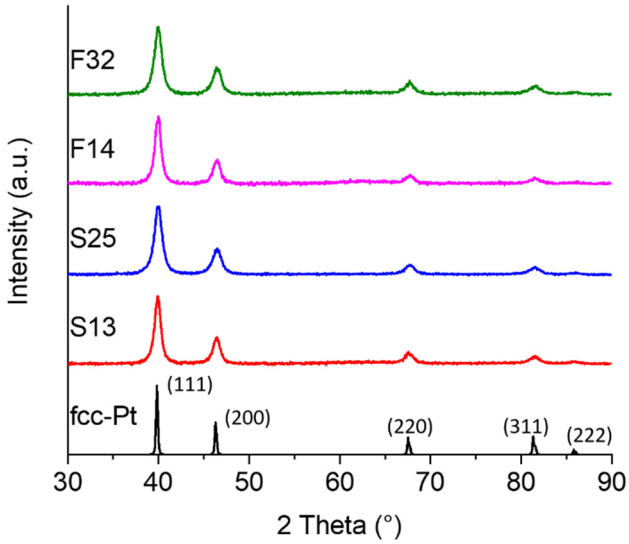

Figure 1. PXRD patterns of selected SC-Pt-NS samples and an fcc-Pt reference (crystallographic open database fcc-Pt: 1011114). The sample designations "S" and "F" indicate the carbohydrate sucrose and fructose, respectively, and the respective number refers to the rounded value of found Pt wt.% from AAS. See Figure S4 for the PXRD patterns of all samples and Table S2 for the average crystallite sizes of the individual samples.

Transmission electron microscopy (TEM) measurements of the sugar-coated Pt nanostructures showed an average size of 8–11 nm for the primary particles, which were aggregated to hierarchical Pt nanostructures of ~65 nm for the Pt/sucrose samples and ~40 nm for the Pt/D(-)-fructose samples (Figure 2). The smaller aggregate sizes for the Pt/D(-)-fructose samples may have been due to the difference between the fructose monosugars, where the equilibrium between the open chain and the furanoic form can play a role. Sucrose is a disaccharide which only upon hydrolysis yields the monomeric building blocks glucose and fructose. This possibly results in more homogenous and smaller aggregates of the primary particles (being of a very similar size in both saccharides) in fructose. In a follow-up study, we plan to further vary the used sugars to investigate their possible role and maybe control in aggregation. The primary particle size from TEM was in good agreement with the crystallite size from the Scherrer equation and PXRD.

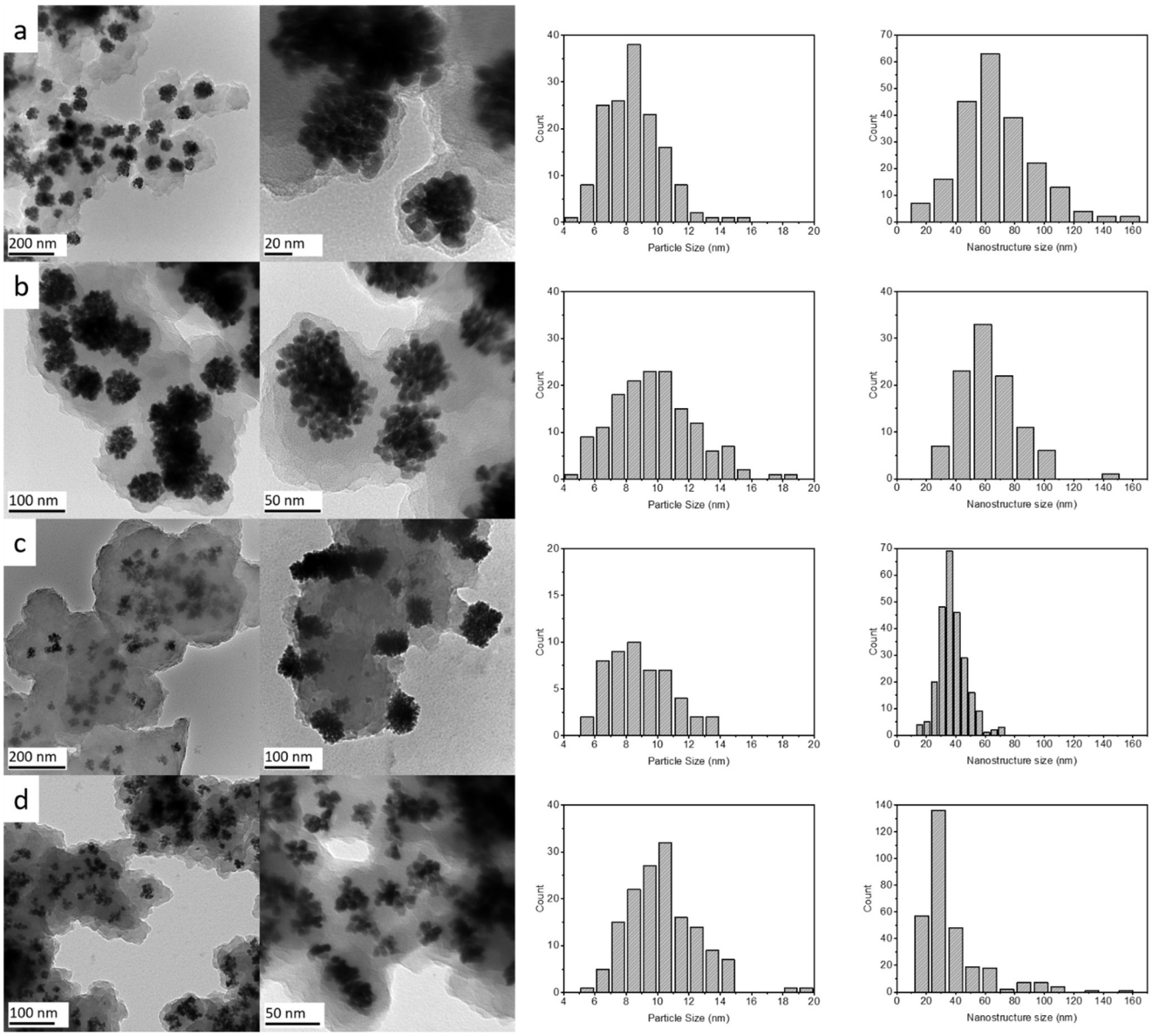

Figure 2. TEM images and histograms for the sizes of the primary particles and the aggregated platinum nanostructures (**a**) S13, with average primary crystallite size of ~9 nm and average aggregated nanostructure size of ~68 nm, (**b**) S25, with sizes of ~8 nm and ~63 nm, (**c**) F14, with sizes of ~11 nm and ~38 nm, and (**d**) F32, with sizes of ~10 nm and ~37 nm, respectively. At least 150 primary particles (except for F14, which showed a high degree of aggregation) and 100 nanostructures were evaluated.

An explanation for the formation of the larger aggregate structures during the synthesis reaction may be the formation of carbohydrate vesicles in the IL, together with the water content of the hexahydrate Pt precursor ($H_2PtCl_6 \cdot 6H_2O$) and water from the dehydration of the carbohydrates [39,40]. As a reducing agent, the saccharide (sugar orcarbohydrate) induces the formation and protection of the primary Pt-NPs, which then assemble to hierarchical structures as part of the carbohydrate vesicle formation or phase separation from the IL. The interaction of the Pt-NPs with the carbohydrate will be stronger compared with the IL, as the latter is known to show only weak coordination with metal nanoparticles through its weakly coordinating cations and anions [8].

We note that water has a negative influence on the nanoparticle stabilization by the IL and thereby promotes the tendency of the primary nanocrystallites to agglomerate in larger structures [33,41]. When $H_2PtCl_6 \cdot 6H_2O$ was reduced in IL with 5 wt.% of water added and

in the absence of a carbohydrate, massively agglomerated nanostructures were formed (Figures S7–S10). This illustrates the stabilizing effect of the carbohydrate in the reaction mixture, which prevents the uncontrolled agglomeration process and forms a protective coating during the synthesis reaction. Consequently, the encapsulated Pt-NS are hindered in their further aggregation.

For comparison, sucrose (S_{sup}) and fructose (F_{sup}) samples without Pt were prepared under the same microwave heating conditions in IL. The effect of the thermal treatment in IL on the carbohydrates was followed by PXRD, elemental analysis, Fourier-transform infrared (FT-IR) spectrometry, thermogravimetric analysis (TGA), nuclear magnetic resonance (NMR), specific optical activity measurements, MALDI-TOF mass spectrometry, gel-permeation/size exclusion chromatography (GPC/SEC) and dynamic light scattering (DLS) (Sections S3–S5 and S8). The PXRD results revealed the expected formation of an amorphous carbohydrate material (Figure S15). The CH analyses (Table S3) gave an increase in the carbon content to ~48% from ~40% and a reduction in the hydrogen content from ~6.7% to ~5.4% compared with the native sugars due to dehydration. Additionally, the CH analyses (Table S3) of the four samples S13, S25, F14 and F32 had a significantly increased carbon-to-hydrogen ratio from ~13.1 to ~14.4, compared with the starting ratios of 6.5 and 5.8 for sucrose and D(-)-fructose, respectively. This supports a partial oxidation and condensation of the saccharide with loss of hydrogen. In addition, the residues of the ionic liquids could be determined from the detected nitrogen and sulfur contents, which could have been enclosed in the carbohydrate nanostructures. The IR spectra (Figure S7) of S_{sup} and F_{sup} indicated a loss of intensities in the fingerprint region compared with the native sugars. Furthermore, a new frequency at ~1700 cm^{-1} can be observed, coinciding with the C=C stretching vibrations. The IR spectra (Figure S7) of the SC-Pt-NS displayed similar peaks as in the thermally treated sugar samples, which included a loss of signals in the fingerprint region compared with the pristine sugars.

TGA measurements (Figure S16) revealed a material stability up to 250 °C. The ^1H NMR spectra of S_{sup} and F_{sup} (Figures S17 and S18) did not show sharp signals compared with the respective carbohydrates; instead, they exhibited broad, unresolved bands in the area of 3.2–5.6 ppm, and IL residues could also be observed. When compared with the pristine sugars (Figures S17 and S18), the NMR signals belonging to sucrose and D(-)-fructose were not detected anymore. These results coincide with a partial dehydration of the carbohydrates and a polymerization to a caramel-like state during their heat treatment, as a caramelization process can occur at 200 °C. Caramel is an ill-defined product from the heat treatment of sugars. During caramelization, chemical processes that are not fully elucidated and sometimes occur simultaneously take place, including a change in mutarotation which, in the case of sucrose, is an inversion. The chemical processes include oxidation, condensation and polymerization reactions, the formation of intramolecular covalent bonds, rearrangements, such as isomerizations and partial pyrolysis, and in the case of darker caramel, increased charring. The sugar is dehydrated, and the carbohydrates combine to form various polymers, ketones and aldehydes. For NMR, the sugar coating was best, albeit not fully soluble in dimethylformamide and dimethylsulfoxide, only very slightly soluble in water and almost insoluble in the organic solvents n-hexane, dichloromethane, acetonitrile and acetone. The broadened IR and NMR signals for the heat-treated samples was due to an inhomogeneous degradation of the carbohydrates.

The specific optical activity of the pristine and thermally treated sugars was measured in dimethylformamide (because of better solubility over water) to be 69°, 49°, −115° and −21° for sucrose, sucrose after heat treatment, D(-)-fructose and D(-)-fructose after heat treatment, respectively. The decrease in optical activity (for the soluble component) agreed with the reaction of the pristine sugar.

MALDI-TOF mass spectrometric measurements (Figures S8–S10) of the SC-Pt-NS samples indicate the formation of oligomeric compounds with m/z ratios of up to 1153 and even somewhat higher m/z ratios for the microwave-heated saccharides in IL. The formation of oligomers was supported by the GPC measurements in dimethylformamide

(Figures S19 and S20) of the saccharides, which showed an M_N of 840 g mol^{-1} and M_W of 1300 g mol^{-1} for sucrose and an M_N of 1020 g mol^{-1} and M_W of 4900 g mol^{-1} for D(-)-fructose after heat treatment. We note that the samples were not completely soluble in the solvent dimethylformamide, so the insoluble polymeric or partially carbonized part from the caramelization process could not be analyzed. The DLS of SC-Pt-NS in chloroform (Figure S6) suggests the formation of hydrodynamic diameters of 330 nm, 300 nm, 1060 nm and 300 nm for the SC-Pt-NS samples S13, S25, F14 and F32, respectively, while S13 also displayed a second (bimodal) hydrodynamic diameter at 5 µm (5000 nm). These findings hint at the formation of similar-sized aggregates and Pt-NS distributions inside each saccharide layer, which also correlated to the aggregates observed in the TEM images (Figure 2). Altogether, these findings let us conclude that the carbohydrates (sugar) were subject to a significant rearrangement, as described in the caramelization process.

3.2. Hydrosilylation Catalysis

The SC-Pt-NS samples were tested as a proof of principle for catalyst activity and separation in the hydrosilylation reaction of phenylacetylene with triethylsilane, where the terminal acetylene function was hydrosilylated with the alkylsilane (Scheme 2). Hydrosilylation reactions [42–46] allow the addition of Si-H bonds to C-C multiple bonds and are of significant importance for green chemistry. For the industrial application of hydrosilylation, the transition metal-catalyzed addition is almost exclusively used. Noble metal catalysts containing Ir, Ru, Pd or the Karstedt and Speier Pt catalysts are widely employed in the silicon industry [47,48]. The exact mechanism for the heterogeneous hydrosilylation reaction with Pt is not well understood yet [46,47,49]. The Chalk–Harrod mechanism [42,47,50,51] for the hydro-silylation reaction is the most accepted reaction mechanism until now, and we assumed that it also applied to our reaction system (Figure S21).

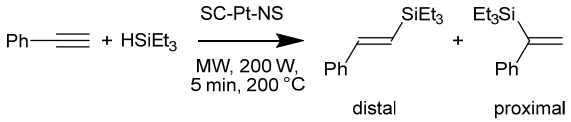

Scheme 2. Hydrosilylation of phenylacetylene with triethylsilane by SC-Pt-NS catalysts, yielding proximal triethyl(1-phenylvinyl)silane and distal (E)-triethyl(styryl)silane (triethyl(2-phenylvinyl)silane).

A challenge for the large-scale production and application of silicones for biomedical materials such as implants is the possible heavy-metal catalyst residues [52,53]. A prominent example that raised high attention was the assumed Pt leakage from breast implants, which was deemed responsible for the "Breast Implant Illness" [54]. Although the severity of the leakage and effect on health are still contested [55], the prevention of catalyst metal impurities in pharmaceutical or medical products is of high importance. Many Pt compounds form catalytically active Pt species in situ in ionic liquids for hydrosilylation [56–60], but the prevention of Pt leakage and material reusability can also be a challenge at a lab scale. The choice of ionic liquid (which was kept constant here but would be another parameter to vary) also shows an important effect on the activity for hydrosilylation [57,58].

The solid SC-Pt-NS sample was placed in a 10-mL glass reactor and mixed with liquid phenylacetylene and triethylsilane under an inert atmosphere. The reactor was subjected to microwave-induced heating at 200 W for 5 min, giving a temperature of 200 °C. Afterward, the color of the sample solution had changed from light yellow to orange, which agreed with previous reports for the hydrosilylation reaction of phenylacetylene with triethylsilane [61]. ^{1}H NMR, ^{13}C NMR and gas chromatographic (GC) analysis allowed us to quantify the conversion and to identify the relative amounts of the proximal triethyl(1-phenylvinyl)silane and distal (E)-triethyl(styryl)silane product species (Sections S9 and S10).

In the literature, the hydrosilylation catalysis is mostly carried out at reaction temperatures below 110 °C, with reaction times between 1.3 and 24 h. While the methods

differ, the reaction times seem to be chosen so as to give high conversion [49,62–66]. The thermal reactions in the literature are longer, but they are carried out in many cases with ppm amounts of Pt precursors. Longer times are not necessarily a problem in larger-scale production. Certainly, thermal Pt-catalyzed hydrosilylation has been well optimized in industry. To the best of our knowledge, microwave heating for hydrosilylation catalysis has been rarely reported [67] or examined in the presence of IL. As such, we also introduce fast and efficient microwave heating, which offers a promising alternative to known batch reactions concerning a reduction in time, which can still be beneficial at the lab scale.

We show that with microwave-induced heating up to 200 °C, conversions of over 98% can be achieved within a very short reaction time of 5 min, significantly faster than in the literature. For comparison, we also tested the Pt precursor $H_2PtCl_6 \cdot 6H_2O$ and sugar-free Pt-NPs in the hydrosilylation reaction under identical conditions. The very short reaction times resulted in remarkably high turnover frequencies (TOFs) of up to 87,200 h^{-1} and 80,300 h^{-1} for the hydrosilylation of phenylacetylene with triethylsilane with sucrose and fructose SC-Pt-NS, respectively (TOF values under footnote 2 in Table 1). In the literature, the TOF values are seldom reported in light of the associated long reaction times of several hours. In Table 1, a comparison to other reaction conditions for the hydrosilylation reaction is presented. It is evident that the SC-Pt-NS catalysts together with the chosen reaction conditions allowed for comparatively very short reaction times of 5 min at very high molar-substrate-to-Pt ratios, with very low amounts of the Pt catalyst and thereby reaching essentially quantitative conversion, which is significantly faster than conventional hydrosilylation catalysis. In addition, after the removal of the Pt catalyst by centrifugation, the amount of Pt metal in the product solution was assessed by AAS exemplarily for the samples S25 and F32. Generally, due to the small scale of the reaction and low amount of Pt-nanostructures used, the detection of Pt inside the product solution is often near the detection limit of a flame AAS or ICP techniques [56,57]. For that reason, we specifically utilized a graphite furnace AAS instead of a flame AAS to quantify even small amounts of platinum in the product solution. The Pt concentrations in the product solutions for samples S25 and F32 were 0.72 mg L^{-1} and 0.93 mg L^{-1}, respectively, which corresponded to leaching of less than 1% of the used amount of Pt (0.7% and 0.9%, respectively) into the product solution, showing that the Pt catalyst could be efficiently removed. We note that leaching of less than 1% of the original catalyst amount into the product solution has been viewed or interpreted in similar work as a successful prevention of leaching [49,64]. In line with the cited literature, we refer to the SC-Pt-NS as a means to successfully prevent leaching. Without separation, the Pt concentration in the product solution would have been 106 mg L^{-1}.

In addition, we performed the reaction without any Pt catalyst. No substrate conversion was detected (Table 1), which shows that microwave irradiation alone had no impact on substrate conversion.

The recovered catalysts were utilized again for the hydrosilylation reaction to examine the reusability. In contrast to our expectations, the SC-Pt-NS showed a significant activity loss after three runs. At the same time, low reusability was also observed for the Pt precursor $H_2PtCl_6 \cdot 6H_2O$ and Pt-NPs obtained under sugar-free conditions. In the post-mortem TEM images of sample S25 after the third catalysis run (Figure S22), a lower degree of aggregation of the primary particles was observed. Additionally, after catalysis, the sugar coating was still present. The two-dimensional TEM images will not show if the saccharide coating fully surrounds the Pt-NPs or if part of the NP surface is exposed. Even if the Pt-NS are fully surrounded, the high temperature of above 200 °C during hydrosilylation will melt the sucrose (mp. 186 °C) or fructose (mp. 103 °C) coating and thereby expose the Pt surface to the reaction medium. Upon cooling, the sugar solidifies again and reestablishes the protective and stabilizing saccharide coating. We also consider catalyst poisoning as possibility, which we will follow up on in subsequent works.

Table 1. Reaction conditions, conversion and distal/proximal ratio of the hydrosilylation of phenylacetylene with triethylsilane.

Catalyst with References	Time (h)	Temp. (°C)	Substrate/Pt [1]	Conversion (%) [2]	d/p Ratio [3]
SC-Pt-NS					
S13	0.083	200	7500	98	2.1
S25	0.083	200	3800	99	1.4
F14	0.083	200	6900	98	1.7
F32	0.083	200	3500	99	1.4
Comparison					
Pt-free [4]	0.083	200	–	0	–
$H_2PtCl_6 \cdot 6H_2O$	0.083	200	2200	98	1.9
Pt-NP	0.083	200	1100	91	1.9
7.0 nm Pt/SBA-15 [62]	6	70	390	6.8	1.8
Pt_1/NaY [49]	24	110	2440	82	0.3
Pt/C [63]	4.5	70	4880	91	3.3
Pt-NP [64]	1.3	60	200	82	4.9
Pt-NP [64]	24	60	200	94	9.0
Pt-NP [65]	10	rt	1000	98	6.7
C-Pt/ImIP-2BrB [66]	4	80	2000	79	0.8

[1] Molar ratio of substrate to Pt content. Substrate amount corresponds to phenylacetylene. A molar ratio of triethylsilane to phenylacetylene of 1.0 was chosen for all reactions with the exception of [49] and [64], where a ratio of 1.2 was utilized. [2] The corresponding TOF values in h^{-1} (turnover frequency ($mol_{product}$ $mol_{Pt}{}^{-1}$ h^{-1})) for samples S13, S25, F14 and F32 are 87,200, 45,600, 80,300 and 41,400, respectively. For $H_2PtCl_6 \cdot 6H_2O$ and Pt-NPs, the TOF values were 25,500 and 11,500 h^{-1}, respectively. [3] Molar ratio of distal to proximal product, determined from ^{1}H NMR spectra of the reaction mixture. [4] The substrates triethylsilane and phenylacetylene were heated as such (i.e., without any catalyst) to determine if microwave irradiation and a high temperature are sufficient to induce the reaction.

A distal/proximal ratio between 1.4 and 1.9 was determined by ^{1}H NMR and confirmed by GC measurements, which revealed similar distal/proximal ratios of 1.3–2.1 (Table S5) of the Supplementary Materials presents the results obtained from the GC experiments. It is noteworthy that the molar distal/proximal product ratio with the SC-Pt-NS catalysts was significantly lower than in most of the comparative literature. Many other Pt-NP catalysts in the literature gave ratios between 3.3 and 9.0 [63–65]. Only Pt_1/NaY [49] and C-Pt/ImIP-2BrB [66] yielded even lower distal/proximal ratios below one (Table 1). For comparison, with $H_2PtCl_6 \cdot 6H_2O$ and sugar-free Pt-NPs, a distal/proximal ratio of 1.9 was obtained in the hydrosilylation reaction under identical conditions, which was similar to the SC-Pt-NS catalysts and suggests that the temperature is a decisive factor for the distal/proximal ratio.

4. Conclusions

We have demonstrated that the agglomeration of nanocrystals, a common phenomenon observed in the synthesis of nanoparticles, can be controlled and stabilized by the formation of a sustainable carbohydrate coating, leading to the formation of hierarchical metal nanostructures by cluster building of well-defined Pt nanocrystals inside the IL vesicles formed during the reaction.

The sugar-coated Pt nanostructures (SC-Pt-NS) achieved very high catalytic activity in the hydrosilylation reaction of phenylacetylene with triethylsilane. Four different SC-Pt-NS catalysts gave over 98% conversion within 5 min, resulting in TOF values of up to 87,200 h^{-1} (for sample S13). A high purity of the product solution was achieved with less than 1% of the Pt species remaining in the product, demonstrating the successful separation of the Pt catalyst and hydrosilylation product. Our findings demonstrate that hierarchical metal nanostructures can be produced by performing direct synthesis using ILs as the reaction medium and carbohydrates as a stabilizing coating material suited for nanostructures, presenting an interesting research field worthy of further examination.

Different from previous works [49,62–66], our study presents a hydrosilylation reaction carried out under microwave-assisted heating, which enables rapid and direct heating of the reaction medium and very short reaction times. In this short reaction time of 5 min, near quantitative conversion was achieved, whereas in previous works, the reaction time was 2 h or more [49,62–66]. Metal nanoparticles can absorb microwave irradiation very well and serve as hot spots [68,69]. As such, microwave heating in the catalysis with Pt nanoparticles can certainly be extended to other reactions to offer an interesting alternative to conventional heating in order to save time.

Supplementary Materials: The following supporting information can be downloaded at https://www.mdpi.com/article/10.3390/chemistry4040078/s1. Section S1: Sources of chemicals; S2: Characterization of the ionic liquid 1-butyl-3-methylimidazoliumbis(trifluoromethylsulfonyl)imide ([BMIm]NTf_2); S3: Synthesis parameters and analyses of sugar-coated platinum nanostructures (SC-Pt-NS) in 1-butyl-3-methyl¬imidazolium-bis(trifluoromethylsulfonyl)imide ([BMIm]NTf_2); S4: Fourier-transform infrared (FTIR) spectroscopy measurements; S5: MALDI-TOF mass spectrometry; S6: Effect of water in the synthesis of platinum nanoparticles in IL; S7: Carbohydrate-free platinum nanoparticles synthesized in 1-butyl-3-methylimidazolium-bis(trifluoromethylsulfonyl)imide ([BMIm]NTf_2); S8: Analysis of thermally treated sugars in IL; S9: Hydrosilylation activity and product analysis; S10: Gas chromatography (GC) analysis. References [42,50,63,70,71] are cited in the supplementary materials.

Author Contributions: Conceptualization, C.J. and J.G.M.-C.; methodology, D.W. (Dennis Woitassek) and J.G.M.-C.; validation, D.W. (Dennis Woitassek); formal analysis, D.W. (Dennis Woitassek); investigation, D.W. (Dennis Woitassek), J.G.M.-C., Y.S. (Yangyang Sun), Y.S. (Yefan Song), D.W. (Dennis Woschko) and S.R.; resources, C.J.; data curation, D.W. (Dennis Woitassek); writing—original draft preparation, D.W. (Dennis Woitassek) and J.G.M.-C.; writing—review and editing, D.W. (Dennis Woitassek) and C.J.; visualization, D.W. (Dennis Woitassek) and J.G.M.-C.; supervision, C.J.; project administration, C.J.; funding acquisition, C.J. All authors have read and agreed to the published version of the manuscript.

Funding: This research was supported by a joint National Natural Science Foundation of China–Deutsche Forschungsgemeinschaft (NSFC-DFG) project (DFG JA466/39-1).

Institutional Review Board Statement: Not applicable.

Informed Consent Statement: Not applicable.

Data Availability Statement: The data presented in this study are available on request from the corresponding author.

Acknowledgments: The authors would like to thank the Center for Molecular and Structural Analytics at Heinrich Heine University (CeMSA@HHU) for recording the mass spectrometric and NMR-spectrometric data. We thank Birgit Tommes, Annette Ricken, Till Strothmann, Stephanie Scheelen and Constantin Czekelius for their help with analysis and synthesis.

Conflicts of Interest: The authors declare that they have no known competing financial interest or personal relationship that could have appeared to influence the work reported in this paper.

References

1. Mizuno, N.; Misono, M. Heterogeneous Catalysis. *Chem. Rev.* **1998**, *98*, 199–218. [CrossRef] [PubMed]
2. Hanefeld, U.; Lefferts, L. (Eds.) *Catalysis: An Integrated Textbook for Students*; Wiley-VCH: Weinheim, Germany, 2018; ISBN 978-3-527-34159-7s.
3. Beller, M.; Renken, A.; van Santen, R.A. (Eds.) *Catalysis: From Principles to Applications*; Wiley-VCH-Verlag GmbH & Co. KGaA: Weinheim, Germany, 2012; ISBN 978-3-527-32349-4.
4. Yazgan, I.; Gümüş, A.; Gökkuş, K.; Demir, M.A.; Evecen, S.; Sönmez, H.A.; Miller, R.M.; Bakar, F.; Oral, A.; Popov, S.; et al. On the Effect of Modified Carbohydrates on the Size and Shape of Gold and Silver Nanostructures. *J. Nanomater.* **2020**, *10*, 1417. [CrossRef] [PubMed]
5. Bera, S.; Mondal, D. A role for ultrasound in the fabrication of carbohydrate-supported nanomaterials. *J. Utrasound* **2019**, *22*, 131–156. [CrossRef] [PubMed]
6. Reverberi, A.P.; Vocciante, M.; Salerno, M.; Soda, O.; Fabiano, B. A sustainable, top-down mechanosynthesis of carbohydrate-functionalized silver nanoparticles. *React. Chem. Eng.* **2022**, *7*, 888–897. [CrossRef]

7. Li, K.; Liu, B. Polymer-encapsulated organic nanoparticles for fluorescence and photoacoustic imaging. *Chem. Soc. Rev.* **2014**, *43*, 6570–6597. [CrossRef]
8. Wegner, S.; Janiak, C. Metal Nanoparticles in Ionic Liquids. *Top. Curr. Chem.* **2017**, *375*, 65. [CrossRef]
9. Dupont, J.; Kollar, L. (Eds.) *Ionic Liquids (ILs) in Organometallic Catalysis*; Topics in Organometallic Chemistry 51; Springer: Berlin/Heidelberg, Germany, 2015; ISBN 978-3-662-47857-8.
10. Xu, D.; Lv, H.; Liu, B. Encapsulation of Metal Nanoparticle Catalysts Within Mesoporous Zeolites and Their Enhanced Catalytic Performances: A Review. *Front. Chem.* **2018**, *6*, 550. [CrossRef]
11. Hosseiniamoli, H.; Bryant, G.; Kennedy, E.M.; Mathisen, K.; Nicholson, D.; Sankar, G.; Setiawan, A.; Stockenhuber, M. Understanding Structure–Function Relationships in Zeolite-Supported Pd Catalysts for Oxidation of Ventilation Air Methane. *ACS Catal.* **2018**, *8*, 5852–5863. [CrossRef]
12. Marquardt, D.; Beckert, F.; Pennetreau, F.; Tölle, F.; Mülhaupt, R.; Riant, O.; Hermans, S.; Barthel, J.; Janiak, C. Hybrid materials of platinum nanoparticles and thiol-functionalized graphene derivatives. *Carbon* **2014**, *66*, 285–294. [CrossRef]
13. Dong, H.; Chen, Y.-C.; Feldmann, C. Polyol synthesis of nanoparticles: Status and options regarding metals, oxides, chalcogenides, and non-metal elements. *Green Chem.* **2015**, *17*, 4107–4132. [CrossRef]
14. Fiévet, F.; Ammar-Merah, S.; Brayner, R.; Chau, F.; Giraud, M.; Mammeri, F.; Peron, J.; Piquemal, J.-Y.; Sicard, L.; Viau, G. The polyol process: A unique method for easy access to metal nanoparticles with tailored sizes, shapes and compositions. *Chem. Soc. Rev* **2018**, *47*, 5187–5233. [CrossRef]
15. Adil, S.F.; Assal, M.E.; Khan, M.; Al-Warthan, A.; Siddiqui, M.R.H.; Liz-Marzán, L.M. Biogenic synthesis of metallic nanoparticles and prospects toward green chemistry. *Dalton Trans.* **2015**, *44*, 9709–9717. [CrossRef]
16. Mittal, A.K.; Chisti, Y.; Banerjee, U.C. Synthesis of metallic nanoparticles using plant extracts. *Biotechnol. Adv.* **2013**, *31*, 346–356. [CrossRef]
17. Sharma, V.K.; Yngard, R.A.; Lin, Y. Silver nanoparticles: Green synthesis and their antimicrobial activities. *Adv. Colloid Interface Sci.* **2009**, *145*, 83–96. [CrossRef]
18. Fievet, F.; Lagier, J.P.; Figlarz, M. Preparing Monodisperse Metal Powders in Micrometer and Submicrometer Sizes by the Polyol Process. *MRS Bull.* **1989**, *14*, 29–34. [CrossRef]
19. Pentsak, E.O.; Galushko, A.S.; Cherepanova, V.A.; Ananikov, V.P. How to Make a Cocktail of Palladium Catalysts with Cola and Alcohol: Heteroatom Doping vs. Nanoscale Morphology of Carbon Supports. *J. Nanomater.* **2021**, *11*, 2599. [CrossRef]
20. Ribeiro, C.A.; Albuquerque, L.J.; de Castro, C.E.; Batista, B.L.; de Souza, A.L.; Albuquerque, B.L.; Zilse, M.S.; Bellettini, I.C.; Giacomelli, F.C. One-pot synthesis of sugar-decorated gold nanoparticles with reduced cytotoxicity and enhanced cellular uptake. *Colloids Surf. A Physicochem. Eng. Asp.* **2019**, *580*, 123690. [CrossRef]
21. Geng, F.; Song, K.; Xing, J.Z.; Yuan, C.; Yan, S.; Yang, Q.; Chen, J.; Kong, B. Thio-glucose bound gold nanoparticles enhance radio-cytotoxic targeting of ovarian cancer. *Nanotechnology* **2011**, *22*, 285101. [CrossRef]
22. Shrivas, K.; Nirmalkar, N.; Thakur, S.S.; Deb, M.K.; Shinde, S.S.; Shankar, R. Sucrose capped gold nanoparticles as a plasmonic chemical sensor based on non-covalent interactions: Application for selective detection of vitamins B1 and B6 in brown and white rice food samples. *Food Chem.* **2018**, *250*, 14–21. [CrossRef]
23. Panigrahi, S.; Kundu, S.; Ghosh, S.; Nath, S.; Pal, T. General method of synthesis for metal nanoparticles. *J. Nanopart. Res.* **2004**, *6*, 411–414. [CrossRef]
24. Panigrahi, S.; Kundu, S.; Ghosh, S.K.; Nath, S.; Pal, T. Sugar assisted evolution of mono- and bimetallic nanoparticles. *Colloids Surf. A Physicochem. Eng. Asp.* **2005**, *264*, 133–138. [CrossRef]
25. Hallett, J.P.; Welton, T. Room-temperature ionic liquids: Solvents for synthesis and catalysis. 2. *Chem. Rev.* **2011**, *111*, 3508–3576. [CrossRef] [PubMed]
26. Welton, T. Ionic liquids in catalysis. *Coord. Chem. Rev.* **2004**, *248*, 2459–2477. [CrossRef]
27. Wender, H.; Migowski, P.; Feil, A.F.; Teixeira, S.R.; Dupont, J. Sputtering deposition of nanoparticles onto liquid substrates: Recent advances and future trends. *Coord. Chem. Rev.* **2013**, *257*, 2468–2483. [CrossRef]
28. Welton, T. Room-Temperature Ionic Liquids. Solvents for Synthesis and Catalysis. *Chem. Rev.* **1999**, *99*, 2071–2084. [CrossRef]
29. Wasserscheid, P.; Keim, W. Ionic Liquids—New "Solutions" for Transition Metal Catalysis. *Angew. Chem. Int. Ed.* **2000**, *39*, 3772–3789. [CrossRef]
30. Consorti, C.S.; Suarez, P.A.Z.; de Souza, R.F.; Burrow, R.A.; Farrar, D.H.; Lough, A.J.; Loh, W.; Da Silva, L.H.M.; Dupont, J. Identification of 1,3-dialkylimidazolium salt supramolecular aggregates in solution. *J. Phys. Chem. B* **2005**, *109*, 4341–4349. [CrossRef]
31. Dupont, J. On the solid, liquid and solution structural organization of imidazolium ionic liquids. *J. Braz. Chem. Soc.* **2004**, *15*, 341–350. [CrossRef]
32. Vollmer, C.; Redel, E.; Abu-Shandi, K.; Thomann, R.; Manyar, H.; Hardacre, C.; Janiak, C. Microwave irradiation for the facile synthesis of transition-metal nanoparticles (NPs) in ionic liquids (ILs) from metal-carbonyl precursors and Ru-, Rh-, and Ir-NP/IL dispersions as biphasic liquid-liquid hydrogenation nanocatalysts for cyclohexene. *Chem. Eur. J.* **2010**, *16*, 3849–3858. [CrossRef]
33. Dupont, J.; Scholten, J.D. On the structural and surface properties of transition-metal nanoparticles in ionic liquids. *Chem. Soc. Rev.* **2010**, *39*, 1780–1804. [CrossRef]
34. Redel, E.; Thomann, R.; Janiak, C. Use of ionic liquids (ILs) for the IL-anion size-dependent formation of Cr, Mo and W nanoparticles from metal carbonyl $M(CO)_6$ precursors. *Chem. Commun.* **2008**, *27*, 1789–1791. [CrossRef]

35. Krämer, J.; Redel, E.; Thomann, R.; Janiak, C. Use of Ionic Liquids for the Synthesis of Iron, Ruthenium, and Osmium Nanoparticles from Their Metal Carbonyl Precursors. *Organometallics* **2008**, *27*, 1976–1978. [CrossRef]
36. Verma, C.; Ebenso, E.E.; Quraishi, M.A. Transition metal nanoparticles in ionic liquids: Synthesis and stabilization. *J. Mol. Liq.* **2019**, *276*, 826–849. [CrossRef]
37. Redel, E.; Krämer, J.; Thomann, R.; Janiak, C. Synthesis of Co, Rh and Ir nanoparticles from metal carbonyls in ionic liquids and their use as biphasic liquid–liquid hydrogenation nanocatalysts for cyclohexene. *J. Organomet. Chem.* **2009**, *694*, 1069–1075. [CrossRef]
38. Cravotto, G.; Gaudino, E.C.; Boffa, L.; Lévêque, J.-M.; Estager, J.; Bonrath, W. Preparation of second generation ionic liquids by efficient solvent-free alkylation of N-heterocycles with chloroalkanes. *Molecules* **2008**, *13*, 149–156. [CrossRef]
39. Jiang, J.; Yu, S.-H.; Yao, W.-T.; Ge, H.; Zhang, G.-Z. Morphogenesis and Crystallization of Bi_2S_3 Nanostructures by an Ionic Liquid-Assisted Templating Route: Synthesis, Formation Mechanism, and Properties. *Chem. Mater.* **2005**, *17*, 6094–6100. [CrossRef]
40. Yee, P.; Shah, J.K.; Maginn, E.J. State of hydrophobic and hydrophilic ionic liquids in aqueous solutions: Are the ions fully dissociated? *J. Phys. Chem. B* **2013**, *117*, 12556–12566. [CrossRef]
41. Redel, E.; Thomann, R.; Janiak, C. First correlation of nanoparticle size-dependent formation with the ionic liquid anion molecular volume. *Inorg. Chem.* **2008**, *47*, 14–16. [CrossRef]
42. Troegel, D.; Stohrer, J. Recent advances and actual challenges in late transition metal catalyzed hydrosilylation of olefins from an industrial point of view. *Coord. Chem. Rev.* **2011**, *255*, 1440–1459. [CrossRef]
43. Alonso, F.; Buitrago, R.; Moglie, Y.; Ruiz-Martínez, J.; Sepúlveda-Escribano, A.; Yus, M. Hydrosilylation of alkynes catalysed by platinum on titania. *J. Organomet. Chem.* **2011**, *696*, 368–372. [CrossRef]
44. Lipke, M.C.; Liberman-Martin, A.L.; Tilley, T.D. Electrophilic Activation of Silicon-Hydrogen Bonds in Catalytic Hydrosilations. *Angew. Chem. Int. Ed.* **2017**, *56*, 2260–2294. [CrossRef] [PubMed]
45. de Almeida, L.D.; Wang, H.; Junge, K.; Cui, X.; Beller, M. Recent Advances in Catalytic Hydrosilylations: Developments beyond Traditional Platinum Catalysts. *Angew. Chem. Int. Ed.* **2021**, *60*, 550–565. [CrossRef] [PubMed]
46. Naganawa, Y.; Inomata, K.; Sato, K.; Nakajima, Y. Hydrosilylation reactions of functionalized alkenes. *Tetrahedron Lett.* **2020**, *61*, 151513. [CrossRef]
47. Nakajima, Y.; Shimada, S. Hydrosilylation reaction of olefins: Recent advances and perspectives. *RSC Adv.* **2015**, *5*, 20603–20616. [CrossRef]
48. Komiyama, T.; Minami, Y.; Hiyama, T. Recent Advances in Transition-Metal-Catalyzed Synthetic Transformations of Organosilicon Reagents. *ACS Catal.* **2017**, *7*, 631–651. [CrossRef]
49. Rivero-Crespo, M.; Oliver-Meseguer, J.; Kapłońska, K.; Kuśtrowski, P.; Pardo, E.; Cerón-Carrasco, J.P.; Leyva-Pérez, A. Cyclic metal(oid) clusters control platinum-catalysed hydrosilylation reactions: From soluble to zeolite and MOF catalysts. *Chem. Sci.* **2020**, *11*, 8113–8124. [CrossRef]
50. Chalk, A.J.; Harrod, J.F. Homogeneous Catalysis. II. The Mechanism of the Hydrosilation of Olefins Catalyzed by Group VIII Metal Complexes 1. *J. Am. Chem. Soc.* **1965**, *87*, 16–21. [CrossRef]
51. Meister, T.K.; Riener, K.; Gigler, P.; Stohrer, J.; Herrmann, W.A.; Kühn, F.E. Platinum Catalysis Revisited—Unraveling Principles of Catalytic Olefin Hydrosilylation. *ACS Catal.* **2016**, *6*, 1274–1284. [CrossRef]
52. Abramov, A.; Diaz Diaz, D. Katalysatoren immobilisieren. *Nachr. Chem.* **2022**, *70*, 75–78. [CrossRef]
53. Lambert, J.M. The nature of platinum in silicones for biomedical and healthcare use. *J. Biomed. Mater. Res. B Appl. Biomater.* **2006**, *78*, 167–180. [CrossRef]
54. Brook, M.A. Platinum in silicone breast implants. *Biomaterials.* **2006**, *27*, 3274–3286. [CrossRef]
55. Wixtrom, R.; Glicksman, C.; Kadin, M.; Lawrence, M.; Haws, M.; Ferenz, S.; Sung, J.; McGuire, P. Heavy Metals in Breast Implant Capsules and Breast Tissue: Findings from the Systemic Symptoms in Women-Biospecimen Analysis Study: Part 2. *Aesthet. Surg. J.* **2022**, *42*, 1067–1076. [CrossRef]
56. Kukawka, R.; Pawlowska-Zygarowicz, A.; Dutkiewicz, M.; Maciejewski, H.; Smiglak, M. New approach to hydrosilylation reaction in ionic liquids as solvent in microreactor system. *RSC Adv.* **2016**, *6*, 61860–61868. [CrossRef]
57. Zielinski, W.; Kukawka, R.; Maciejewski, H.; Smiglak, M. Ionic Liquids as Solvents for Rhodium and Platinum Catalysts Used in Hydrosilylation Reaction. *Molecules.* **2016**, *21*, 1115. [CrossRef]
58. Geldbach, T.J.; Zhao, D.; Castillo, N.C.; Laurenczy, G.; Weyershausen, B.; Dyson, P.J. Biphasic hydrosilylation in ionic liquids: A process set for industrial implementation. *J. Am. Chem. Soc.* **2006**, *128*, 9773–9780. [CrossRef]
59. Taccardi, N.; Fekete, M.; Berger, M.E.; Stanjek, V.; Schulz, P.S.; Wasserscheid, P. Catalyst recycling in monophasic Pt-catalyzed hydrosilylation reactions using ionic liquids. *Appl. Catal. A Gen.* **2011**, *399*, 69–74. [CrossRef]
60. Hofmann, N.; Bauer, A.; Frey, T.; Auer, M.; Stanjek, V.; Schulz, P.S.; Taccardi, N.; Wasserscheid, P. Liquid-Liquid Biphasic, Platinum-Catalyzed Hydrosilylation of Allyl Chloride with Trichlorosilane using an Ionic Liquid Catalyst Phase in a Continuous Loop Reactor. *Adv. Synth. Catal.* **2008**, *350*, 2599–2609. [CrossRef]
61. Marquardt, D.; Barthel, J.; Braun, M.; Ganter, C.; Janiak, C. Weakly-coordinated stable platinum nanocrystals. *CrystEngComm* **2012**, *14*, 7607–7615. [CrossRef]

62. Dobó, D.G.; Sipos, D.; Sápi, A.; London, G.; Juhász, K.; Kukovecz, Á.; Kónya, Z. Tuning the Activity and Selectivity of Phenylacetylene Hydrosilylation with Triethylsilane in the Liquid Phase over Size Controlled Pt Nanoparticles. *Catalysts* **2018**, *8*, 22. [CrossRef]
63. Chauhan, M.; Hauck, B.J.; Keller, L.P.; Boudjouk, P. Hydrosilylation of alkynes catalyzed by platinum on carbon. *J. Organomet. Chem.* **2002**, *645*, 1–13. [CrossRef]
64. Fernández, G.; Pleixats, R. Soluble Pt Nanoparticles Stabilized by a Tris-imidazolium Tetrafluoroborate as Efficient and Recyclable Catalyst for the Stereoselective Hydrosilylation of Alkynes. *ChemistrySelect* **2018**, *3*, 11486–11493. [CrossRef]
65. Chauhan, B.P.S.; Sarkar, A. Functionalized vinylsilanes via highly efficient and recyclable Pt-nanoparticle catalysed hydrosilylation of alkynes. *Dalton Trans.* **2017**, *46*, 8709–8715. [CrossRef] [PubMed]
66. Fang, H.; Chen, J.; Xiao, Y.; Zhang, J. Platinum nanoparticles confined in imidazolium-based ionic polymer for assembling a microfluidic reactor with enhanced catalytic activity. *Appl. Catal. A: Gen.* **2019**, *585*, 117186. [CrossRef]
67. Hu, W.; Xie, H.; Yue, H.; Prinsen, P.; Luque, R. Super-microporous silica-supported platinum catalyst for highly regioselective hydrosilylation. *Catal. Commun.* **2017**, *97*, 51–55. [CrossRef]
68. Tierney, J.P.; Lidström, P. *Microwave Assisted Organic Synthesis*; Blackwell Publishing: Oxford, UK, 2005. [CrossRef]
69. Hill, J.M.; Marchant, T.R. Modelling microwave heating. *Appl. Math. Model.* **1996**, *20*, 3–15. [CrossRef]
70. Max, J.-J.; Chapados, C. Glucose and fructose hydrates in aqueous solution by IR spectroscopy. *J. Phys. Chem. A* **2007**, *111*, 2679–2689. [CrossRef] [PubMed]
71. Yong, L.; Kirleis, K.; Butenschön, H. Stereodivergent Formation of Alkenylsilanes:syn oranti Hydrosilylation of Alkynes Catalyzed by a Cyclopentadienylcobalt(I) Chelate Bearing a Pendant Phosphane Tether. *Adv. Synth. Catal.* **2006**, *348*, 833–836. [CrossRef]